Solar Phys (2014) 289:1101–1113
DOI 10.1007/s11207-013-0383-8

Time-Series Analysis of Supergranule Characteristics at Solar Minimum

Peter E. Williams · W. Dean Pesnell

Received: 15 September 2012 / Accepted: 2 August 2013 / Published online: 28 August 2013

Abstract Sixty days of Doppler images from the *Solar and Heliospheric Observatory* (SOHO) / *Michelson Doppler Imager* (MDI) investigation during the 1996 and 2008 solar minima have been analyzed to show that certain supergranule characteristics (size, size range, and horizontal velocity) exhibit fluctuations of three to five days. Cross-correlating parameters showed a good, positive correlation between supergranulation size and size range, and a moderate, negative correlation between size range and velocity. The size and velocity do exhibit a moderate, negative correlation, but with a small time lag (less than 12 hours). Supergranule sizes during five days of co-temporal data from MDI and the *Solar Dynamics Observatory* (SDO) / *Helioseismic Magnetic Imager* (HMI) exhibit similar fluctuations with a high level of correlation between them. This verifies the solar origin of the fluctuations, which cannot be caused by instrumental artifacts according to these observations. Similar fluctuations are also observed in data simulations that model the evolution of the MDI Doppler pattern over a 60-day period. Correlations between the supergranule size and size range time-series derived from the simulated data are similar to those seen in MDI data. A simple toy-model using cumulative, uncorrelated exponential growth and decay patterns at random emergence times produces a time-series similar to the data simulations. The qualitative similarities between the simulated and the observed time-series suggest that the fluctuations arise from stochastic processes occurring within the solar convection zone. This behavior, propagating to surface manifestations of supergranulation, may assist our understanding of magnetic-field-line advection, evolution, and interaction.

P.E. Williams (✉)
Department of Physics, Northern Virginia Community College, Annandale, VA, USA
e-mail: pewilliams@nvcc.edu

P.E. Williams
Catholic University of America, Washington, DC, USA

P.E. Williams · W.D. Pesnell
Code 671, NASA Goddard Space Flight Center, Greenbelt, MD, USA

Keywords Sun: convection · Dopplergrams · Helioseismology · Sun: photosphere · SOHO/MDI · SDO/HMI · Solar cycle · Solar minimum · Solar dynamo · Sun: supergranulation

1. Introduction

Irregularities in the measured rotation rate of the Sun were noticed in the early 1900s, but were attributed to observer bias (see, *inter alia*, Plaskett and Delury, 1913; Plaskett, 1916). Hart (1956) showed that the fluctuations were solar in origin and had scale lengths of $\approx 26\,000$ km. It was the use of spectroheliograms by Leighton, Noyes, and Simon (1962) that allowed the Doppler velocity to be measured across the disk of the Sun and showed that these velocities formed the cellular patterns we call supergranules (see the review by Rieutord and Rincon, 2010).

Supergranulation cells have lifetimes of one to two days and are typically ≈ 30 Mm across, but the range of sizes can be quite large (Meunier *et al.*, 2007; Rieutord *et al.*, 2010). Table 1 summarizes the findings of Williams and Pesnell (2011a). It was found that during both the most recent solar minima (that concluded Solar Cycles 22 and 23, respectively) supergranulation cells were on the order of 35 Mm across. Using the upper and lower boundaries of the FWHM of the supergranule feature in the cell-size distribution spectrum, a size range between 19 – 65 Mm was estimated. Previously, Hathaway *et al.* (2000) produced size distributions of Doppler patterns within high-resolution *Michelson Doppler Imager* (MDI) images that exhibit a crossover between the supergranule and granule components. This suggests that the lower limit of supergranulation cell sizes may extend to below 10 Mm, similar in size to the largest granules.

Supergranules are well-known for their low radial velocities and strong divergent horizontal surface-flows. By isolating the spectral power at supergranule wavenumbers, thus removing the velocity contributions from granulation, Williams and Pesnell (2011a) found the radial and horizontal velocities to be around 8 $\mathrm{m\,s^{-1}}$ and 140 $\mathrm{m\,s^{-1}}$, respectively (Table 1). Although it seems that little heat is convected by these cells, reflected in the observed weak center-to-edge temperature gradient of photospheric supergranulation cells (Meunier, Roudier, and Rieutord, 2008; Goldbaum *et al.*, 2009), they certainly play a role in dragging magnetic-field lines to the surface and advecting them to cell boundaries.

While the aforementioned studies of the long-term, inter-year variation of supergranulation characteristics exist, studies at much shorter timescales are rarer. We have extended our studies (Williams and Pesnell, 2011a) of supergranulation characteristics (such as sizes, size ranges, and velocities) at solar minimum to provide a better error- and statistical analysis of our data, and in doing so have observed fluctuations in these characteristics with periods of three to five days (Williams and Pesnell, 2011b). This article describes the observation and subsequent analysis of the time-series of these properties and any correlations among them, and also determines whether the sources of the fluctuations are instrumental or solar.

2. Data Preparation

The *Michelson Doppler Imager* (MDI: Scherrer *et al.*, 1995), launched onboard the *Solar and Heliospheric Observatory* (SOHO) in 1996, has performed a yearly dynamics run of approximately 60 days during which full-disk 1024×1024 Dopplergrams were transmitted to the ground. These $2''$ $\mathrm{pixel^{-1}}$ resolution image data contain line-of-sight photospheric

Table 1 Comparison of time-averaged supergranule parameters between the minima of Solar Cycles 22/23 and 23/24.

Parameter	Symbol	Units	1996 Mean	2008 Mean
Spectral peak wavenumber	$\ell_{\rm peak}$		122 ± 1	125 ± 1
Spectral peak FWHM	$\Delta\ell$		155 ± 3	164 ± 4
Supergranule diameter	λ	Mm	35.9 ± 0.3	35.0 ± 0.3
Radial velocity	$V_{\rm r}$	$\mathrm{m\,s^{-1}}$	7.6 ± 1.4	7.5 ± 1.6
Horizontal velocity	$V_{\rm h}$	$\mathrm{m\,s^{-1}}$	139 ± 1	141 ± 1
1/e Lifetime	$\tau_{1/e}$	h	17.8 ± 0.5	17.7 ± 0.4
Number of supergranules	$N_{\rm SG}$		6005	6318

velocities obtained from the Ni I 6767 Å line at a one-minute cadence. These images have been analyzed to produce an array of results that include helioseismic studies of the internal differential rotation profile (Schou *et al.*, 1998) and determinations of subsurface flows using methods such as ring-diagram and time–distance analyses (Hindman *et al.*, 2004).

For our studies of supergranulation, these images require processing to remove the Doppler signals caused by the five-minute *p*-mode oscillations that have spatial scales similar to supergranules. The removal process (Hathaway, 1988b) involves averaging 31 Gaussian-weighted Dopplergrams that were derotated to the rotational phase of the central image. The resulting averages are then sampled every 15 minutes, producing 96 Doppler images per day.

The SOHO spacecraft orbits around the L_1 Lagrangian point situated at the point of gravitational balance between the Sun and the Earth. Along with the yearly orbital motion around the Sun, the velocity signal due to the spacecraft's motion around L_1 needs to be removed from the Dopplergrams. Furthermore, the gravitational redshift velocity component is also subtracted.

Finally, the axisymmetric flows, such as differential rotation, meridional flow and convective blueshift, are removed. The method, described by Hathaway (1992), involves fitting the flow profiles by calculating the coefficients of a spherical-harmonic series that are summed to give the velocity profile of each flow and then subtracting that profile from the image. After also removing any instrumental artifacts, the resulting image contains velocity signals due only to photospheric manifestations of solar convection. An additional step during this process involves remapping the image to heliographic coordinates (Thompson, 2002), linear in both latitude and longitude.

3. Data Analyses

We applied analysis methods similar to those used by Williams and Pesnell (2011a) to calculate from each processed Doppler image the globally averaged supergranule spectral peak wavenumber [$\ell_{\rm peak}$] and the FWHM [$\Delta\ell$], from which the supergranule size and size range can be derived, as well as the horizontal-velocity component [$V_{\rm h}$]. Data between 25 May and 23 July 1996 (MDI day 1240 – 1299) and 3 March and 1 May 2008 (MDI day 5540 – 5599) were analyzed.

To determine $\ell_{\rm peak}$ and $\Delta\ell$, a modified Lorentzian was used to fit the supergranule feature of the power spectrum derived from each heliographic Doppler map. Spectral amplitudes [A_ℓ^m] in spherical harmonic degree [ℓ] and order [m] were derived by projecting the maps

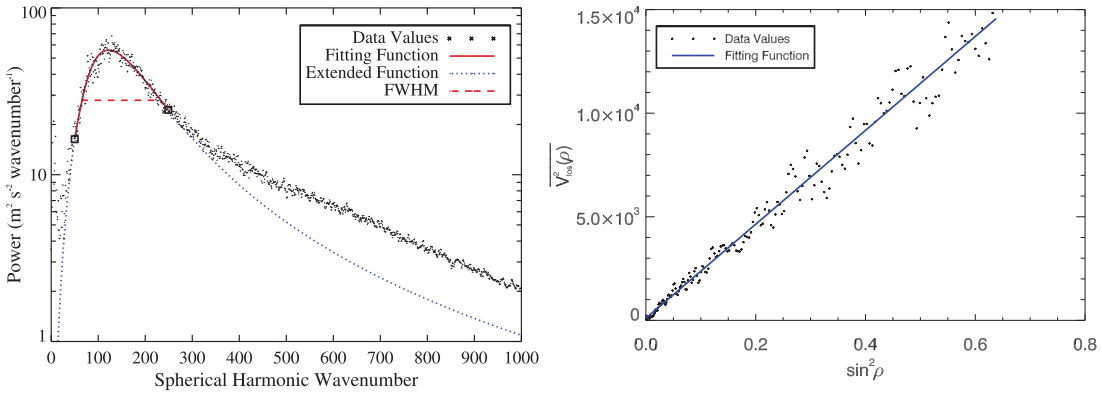

Figure 1 Analysis plots of a single MDI Dopplergram from 27 April 2008, 00:00 UT. (Left) A power spectrum derived from a Doppler image (black dots) is fitted with a modified Lorentzian (solid red line). From this, ℓ_{peak} and $\Delta\ell$ (signified by the FWHM, dashed red line) are determined. The full function is plotted for context (dotted blue line). (Right) Average values of the squared velocities of pixels within each annulus at an angular distance [ρ] from disk center are plotted against $\sin^2\rho$. The horizontal velocity [V_{h}] is determined from the fit.

onto the spherical harmonics (Hathaway *et al.*, 2000). The power spectrum in ℓ was then produced by summing over m:

$$P(\ell) = \sum_{m=-\ell}^{\ell} \left|A_\ell^m\right|^2. \tag{1}$$

The supergranule feature, as seen in Figure 1 (left) peaking at around $\ell = 120$, is fitted between $50 \leq \ell \leq 250$ with a modified Lorentzian,

$$f(\ell) = \left\{\frac{\ell A}{[(\ell - \ell_0)^2 + \Gamma^2]}\right\}^2, \tag{2}$$

from which ℓ_{peak} is derived from the peak of the fitting function and $\Delta\ell$ from its FWHM.

The horizontal velocities [V_{h}] were determined from each heliocentric Dopplergram by dividing the image into a set of concentric annuli of an angular distance [ρ] from disk center and then determining the average of the squared velocities at each pixel contained within (Hathaway *et al.*, 2002). Plotting the average value within each annulus against $\sin^2\rho$ produces a straight line (Figure 1, right) from which V_{h} can be calculated from the slope and intercept values using

$$\overline{V^2(\rho)} = \overline{V_{\text{r}}^2} + \left(\overline{V_{\text{h}}^2} - \overline{V_{\text{r}}^2}\right)\sin^2\rho\,. \tag{3}$$

However, to properly determine V_{h} throughout the time-series, Doppler image pixels within regions of high magnetic activity must be removed because spurious velocity values are measured in these regions (Liu and Norton, 2001). We used contemporaneous 96-minute cadence MDI magnetograms to mask out Dopplergram pixels, correlating to magnetogram pixels with line-of-sight magnetic fields above 25 Gauss. We then used morphological open and close algorithms to mask out pixels over a large area to make sure that any spurious velocity values not matching the original mask were also masked out. We then applied the horizontal-velocity calculations to each individual Dopplergram.

The resulting data consist of three 15-minute-cadence time-series for each of the quantities analyzed. The mean and standard deviation for each time-series is calculated and shown in Table 2.

Table 2 Comparison of supergranule parameters between the solar minima of Cycles 22/23 and 23/24 determined by averaging over the 15-minute-cadence time-series. While the mean values are similar to those in Table 1, the error estimates are now represented by the standard deviations of the datasets.

Parameter	Symbol	Units	1996 Mean	2008 Mean
Spectral peak wavenumber	$\ell_{\rm peak}$		122 ± 1	125 ± 2
Spectral peak FWHM	$\Delta\ell$		156 ± 7	164 ± 9
Horizontal velocity	$V_{\rm h}$	$\mathrm{m\,s^{-1}}$	139 ± 3	141 ± 3

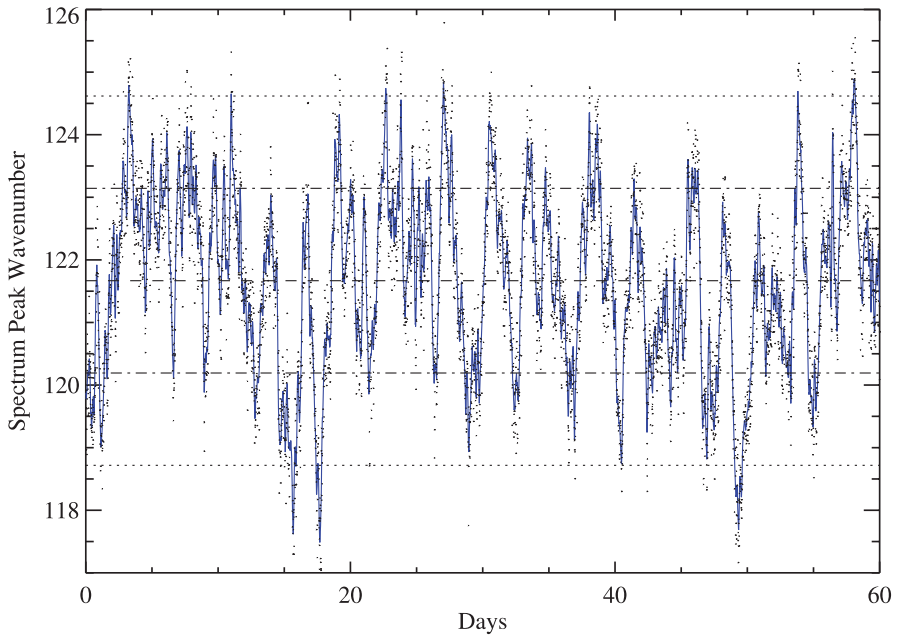

Figure 2 A time-series of $\ell_{\rm peak}$ calculated from the spectra derived from the set of 1996 Dopplergrams. Each 15-minute $\ell_{\rm peak}$ value is represented by a black dot. The dashed line corresponds to a mean value $\overline{\ell}_{\rm peak} = 121.7$, the dot–dashed and dotted lines are the 1σ and 2σ values, respectively, where $\sigma = 1.5$. The blue line is due to smoothing the time-series with a 33-point-wide Savitzky–Golay filter that retains much of the variation of the original time-series.

An example time-series for $\ell_{\rm peak}$ is shown in Figure 2 along with the values for the mean [$\overline{\ell}_{\rm peak} = 121.7$] and standard deviation [$\sigma = 1.5$]. The time-series exhibits fluctuations with a period of around four days, which were investigated by means of frequency analysis. Firstly, the data were smoothed using a fourth-degree zeroth-order 33-point-wide Savitzky–Golay filter (overplotted in Figure 2). The mean was subtracted and low-frequency trends were removed by subtracting a version of the original time-series that was smoothed with a five-day boxcar function. These trends were not investigated because the current work focuses on the four-day periodicities. After padding the ≈ 6000 point data-series to 8192 points to reduce aliasing and normalizing to a standard deviation of one, a fast Fourier transform (FFT) was applied, resulting in the frequency spectra shown in Figure 3. The window function illustrating the resolution of the frequency analysis is shown as a dashed black line. The frequency distribution in Figure 3a relates to the time-series of Figure 2. Dominant peaks are seen at around 0.25 and 0.35 cycles per day. Peaks at similar frequencies (and thus similar periods) are also seen in the 2008 data (Figure 3b). Fourier analyses were also applied to the 1996 and 2008 time-series for $\Delta\ell$ and $V_{\rm h}$ with similar results (Figure 3c – f). These show that

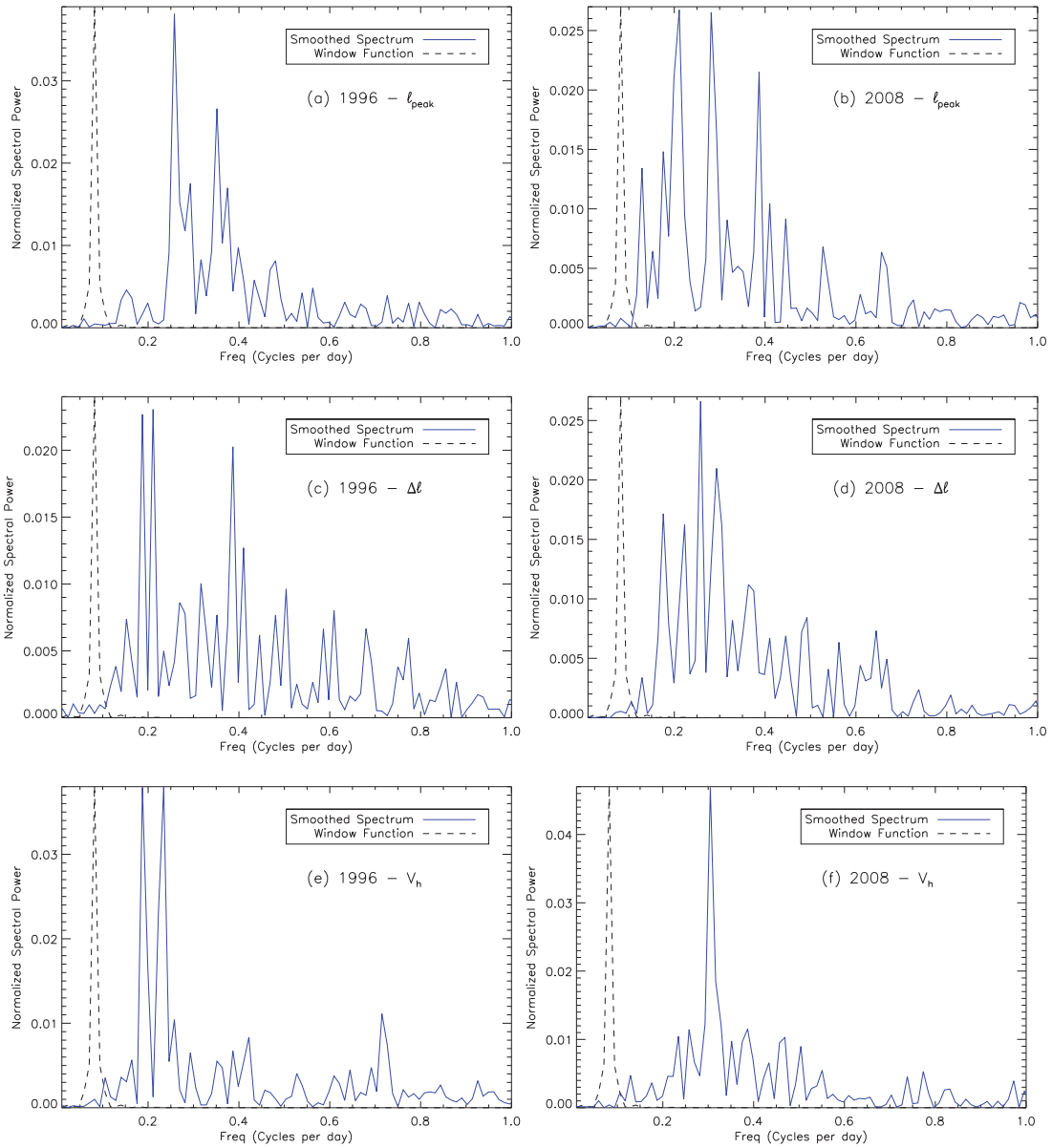

Figure 3 All of the filtered time-series are de-trended, have their means removed, are padded to 8192 points, and normalized to a standard deviation equal to unity before applying an FFT. The resulting 1996 (a, c, e) and 2008 (b, d, f) power spectra (solid blue line) are plotted for the supergranule characteristics ℓ_{peak}, $\Delta\ell$, and V_{h}, respectively. A plot of the window function (dashed black line) is added, representing the resolution of the frequency analysis and peaking at an arbitrary frequency for clarity.

there seems to be an underlying time-dependent fluctuation for each of these characteristics of around 0.2 – 0.4 cycles per day, relating to periods of around three to five days.

4. Inter-Characteristic Comparisons

With the observed fluctuations in the time-variation of each of the supergranule characteristics, it is worth investigating any correlation between them. The Pearson correlation coefficient, which parameterizes their mutual correlation, was calculated for each time-series

Table 3 Comparison of time-averaged supergranule parameters between the solar minima of Cycles 22/23 and 23/24.

Quantity	Characteristics	1996	2008
Pearson correlation coefficient	$R_{\ell_{\rm peak},\Delta\ell}$	0.41	0.48
	$R_{\ell_{\rm peak},V_{\rm h}}$	−0.03	−0.10
	$R_{\Delta\ell,V_{\rm h}}$	−0.21	−0.30
Hurst exponent	$\ell_{\rm peak}$	0.76	0.80
	$\Delta\ell$	0.82	0.82
	$V_{\rm h}$	0.76	0.80

pair. For two arbitrary time-series $[x]$ and $[y]$ consisting of N_x and N_y values $[x_i]$ and $[y_i]$, the Pearson coefficient for the correlated pair $[R_{x,y}]$ is calculated from

$$R_{x,y} = \frac{1}{n-1}\sum_{i=1}^{n}\left(\frac{x_i-\overline{x}}{\sigma_x}\right)\left(\frac{y_i-\overline{y}}{\sigma_y}\right), \tag{4}$$

where $\overline{x}$, $\overline{y}$, $\sigma_{x,}$ and σ_y are the means and standard deviations of the x and y time-series, respectively. Note that the time-series components for this calculation include points for which values exist at the same time in both series. If no point exists at a certain time in either series, the points were removed from the calculation.

The Pearson coefficients for each parameter pair for both datasets are listed in Table 3. They show that the spectral peak wavenumber (inversely proportional to the globally averaged supergranule size) and the spectral FWHM, the supergranule size-range, are moderately correlated at $R_{\ell_{\rm peak},\Delta\ell} = 0.41$ for 1996 and $R_{\ell_{\rm peak},\Delta\ell} = 0.48$ for 2008, while the peak wavenumber and horizontal velocity are poorly correlated, suggesting no relation between these two quantities with $R_{\ell_{\rm peak},V_{\rm h}} = -0.03$ for 1996 and $R_{\ell_{\rm peak},V_{\rm h}} = -0.10$ for 2008. However, the supergranule size range and horizontal velocity show a weak correlation, with $R_{\Delta\ell,V_{\rm h}} = -0.21$ for 1996 and $R_{\Delta\ell,V_{\rm h}} = -0.30$ for 2008. Figure 4 shows a set of scatter plots illustrating the time-series pair correlations. The mean value and 1σ and 2σ values for each time-series are also shown.

To consider the possibility of phase shifts between the correlated pairs, the central 30 days of the first time-series were selected, then the Pearson coefficient calculated over a series of lag-times (between ± 15 days) with the second time-series. Figure 5 shows the change in the Pearson coefficient over the range of lag-times for each parameter pair. The plots show that the correlation between $\ell_{\rm peak}$ and $\Delta\ell$ is strongest at zero time-lag, showing that there is no lag between the quantities and suggesting one quantity does not influence another. Both these quantities seem to be roughly anti-correlated with $V_{\rm h}$ and exhibiting an element of lag. With $\ell_{\rm peak}$ being anti-correlated to $V_{\rm h}$ and inversely proportional to the supergranule size, the results suggest a direct correlation between supergranule size and horizontal velocity. This matches previous findings (Meunier *et al.*, 2007).

These resulting inter-correlations could be caused by the size parameters being derived from the same analysis process while a different process was used to derive the velocities. They also show fluctuations in the Pearson coefficients with periods similar to the fluctuations of the time-series themselves. This is very noticeable in the 2008 data, where fluctuations in the correlation coefficient of around 3.5 days are apparent.

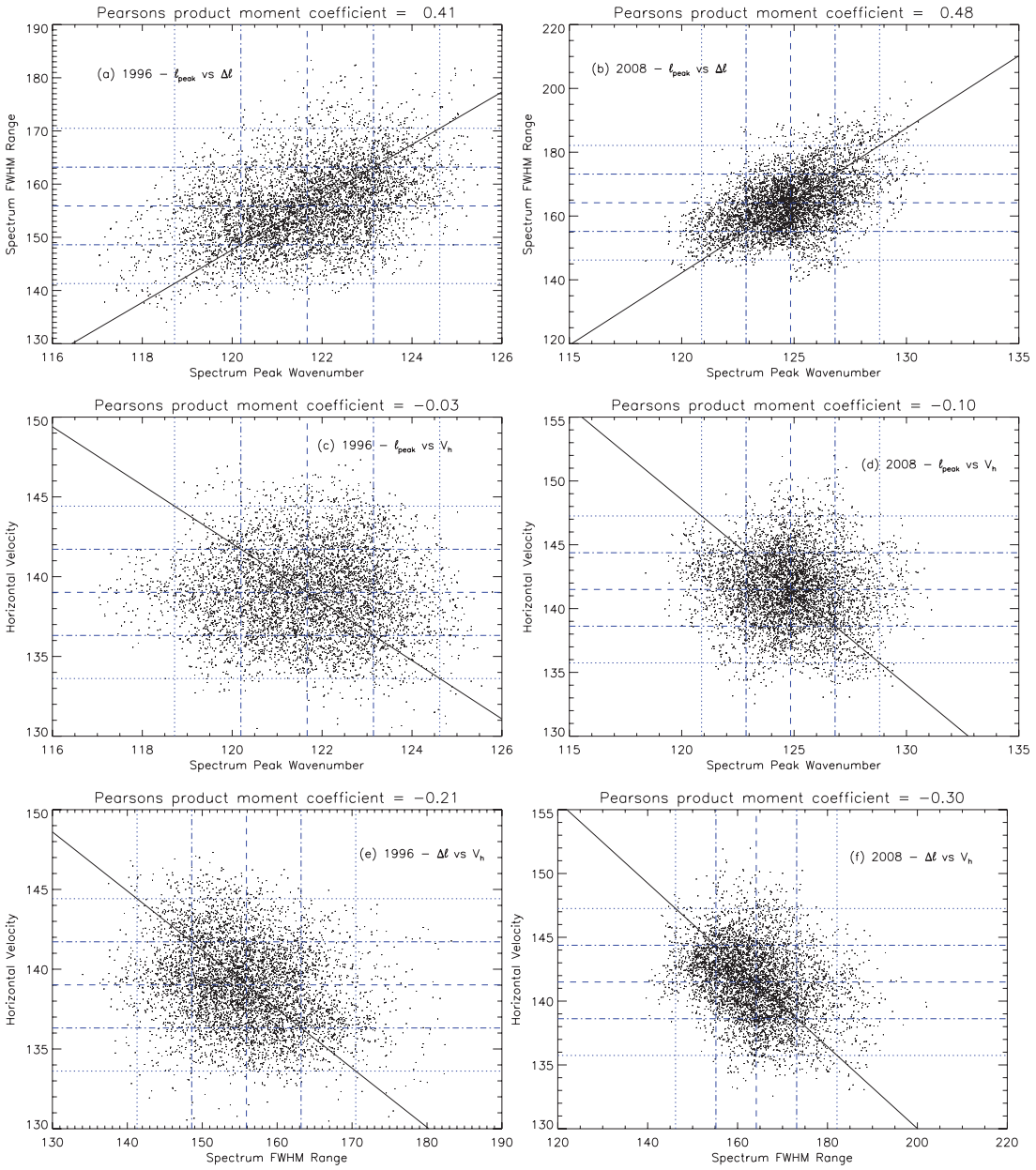

Figure 4 Scatter plots illustrating the correlations between the 60-day time-series of supergranule characteristics for 1996 (left column) and 2008 (right column). The plots correspond to the Pearson coefficients $R_{\ell_{\rm peak},\Delta\ell}$ (top), $R_{\ell_{\rm peak},V_{\rm h}}$ (middle) and $R_{\Delta\ell,V_{\rm h}}$ (bottom), respectively. The dashed, dot–dashed, and dotted lines relate to respective the mean, 1σ, and 2σ values for each time-series.

5. Additional Analyses

To quantify any stochastic element of the fluctuations, and thus a level of predictability, the Hurst exponent (Mandelbrot and Wallis, 1969; Pesnell, 2012) was determined for each of the six time-series. A value of around 0.5 relates to a pure random walk, while a value toward unity defines fully predictable time-series. Table 3 lists the calculated Hurst exponents, indicating some predictability within the time-series.

To investigate whether the observed fluctuations are solar in origin or are due to instrumental artifacts of MDI, such as defocusing (Korzennik, Rabello-Soares, and Schou, 2004;

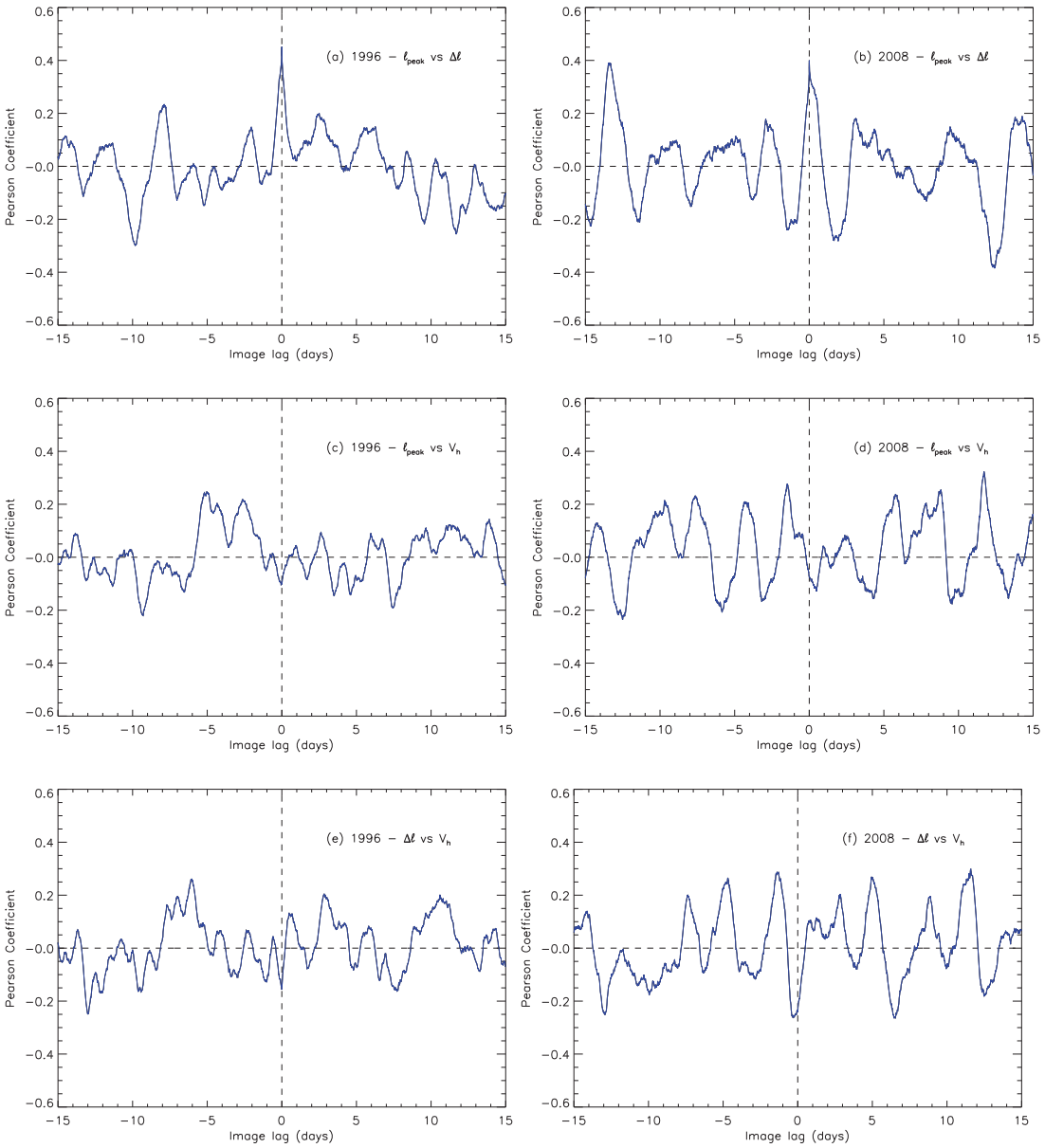

Figure 5 Dependence of correlation values on lag-times between two 30-day selections from time-series pairs from 1996 and 2008. Note that the zero time-lag correlation values are different from those of Figure 4, which were calculated with the full 60-day time-series.

Williams and Pesnell, 2011a), contemporaneous Dopplergrams taken between 6 and 10 July 2010 by both MDI and HMI were analyzed and compared. Plotting the time-series of ℓ_{peak} obtained from both datasets (Figure 6, left) illustrates very similar trending. Note that the discrepancy in the mean values is caused by the different resolution of the instruments (Williams *et al.*, 2013). Correlating the data sets (Figure 6, right) results in a Pearson coefficient of 0.78, indicating a very good correlation. This highlights that the same fluctuating phenomenon was observed in both instruments and allows us to conclude that the fluctuations have a solar origin.

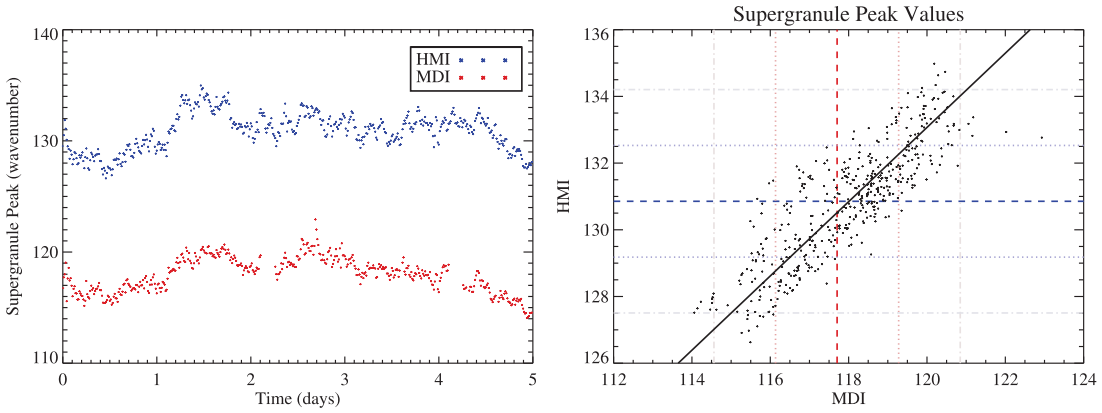

Figure 6 (Left) Time-series of ℓ_{peak} derived from contemporaneous MDI (red) and HMI (blue) Dopplergrams covering the time range 6 – 10 July 2010. (Right) Scatter plot representing the correlation between the MDI and HMI time-series. The Pearson correlation coefficient is 0.78.

6. Computer Simulations

The fluctuations were reproduced in simulated data with the aim of shedding more light on their origins. Simulations that produce realistic Doppler images (Hathaway, 1988a; Hathaway *et al.*, 2010) were used to produce 60 days of images at a 15-minute cadence. The images were produced from a synthetic input spectrum containing both supergranule and granule components. These provide the spectral amplitudes for the orthogonal velocity elements that are constructed with the use of the spherical harmonics, which in turn were combined and projected onto the line of sight. The simulation algorithm advects the Doppler pattern according to differential rotation and meridional circulation profiles, the former advecting the cells at rates relative to their size, *i.e.* dependent on the depths at which they are anchored. Their physical size also determines the rate at which the cells evolve.

The simulated dataset was then processed to remove the axisymmetric-flow signals, mapped to heliographic coordinates and projected onto the spherical harmonics from which the spectral amplitudes were extracted. From these, we produced power spectra and calculated the supergranule-feature peak wavenumber and widths. Figure 7 (top-left) shows the temporal distribution of the peak wavenumbers, showing fluctuations that seem to have a higher frequency than those seen in the real data. This is highlighted in the spectrum (Figure 7, top-right) of the time-series, where a prominent peak is observed at 0.5 cycles per day, *i.e.* a periodicity of two days. This is shorter than that observed in the MDI results, possibly due to the input function that determines the evolution of the convective Doppler pattern that overcompensates for smaller, shorter-lived features. These features tend to dominate the time-series, which is reflected in the power spectrum. This overcompensation is seen when comparing the decay of the synthetic Doppler signal with that from MDI, in particular at low time-lags. This is also seen at high time-lags, but by this time the longer-lived pattern is a much weaker component of the pattern as a whole, and so the short-lived signal is more dominant within the time-series and the related spectra. While this difference in periodicity between the observed and simulated time-series could be explained by the decay rate of the Doppler signal (Figure 7, bottom-left), which is an element of the simulation to be analyzed in future work, that the fluctuations are observed in simulated data with no hydrodynamical influence whatsoever suggests that they arise from the evolution of the Doppler signal itself. A similar trend is seen within a time-series of the FWHM values. The subsequently calculated value of the correlation coefficient relating the two time-series (Figure 7, bottom-right)

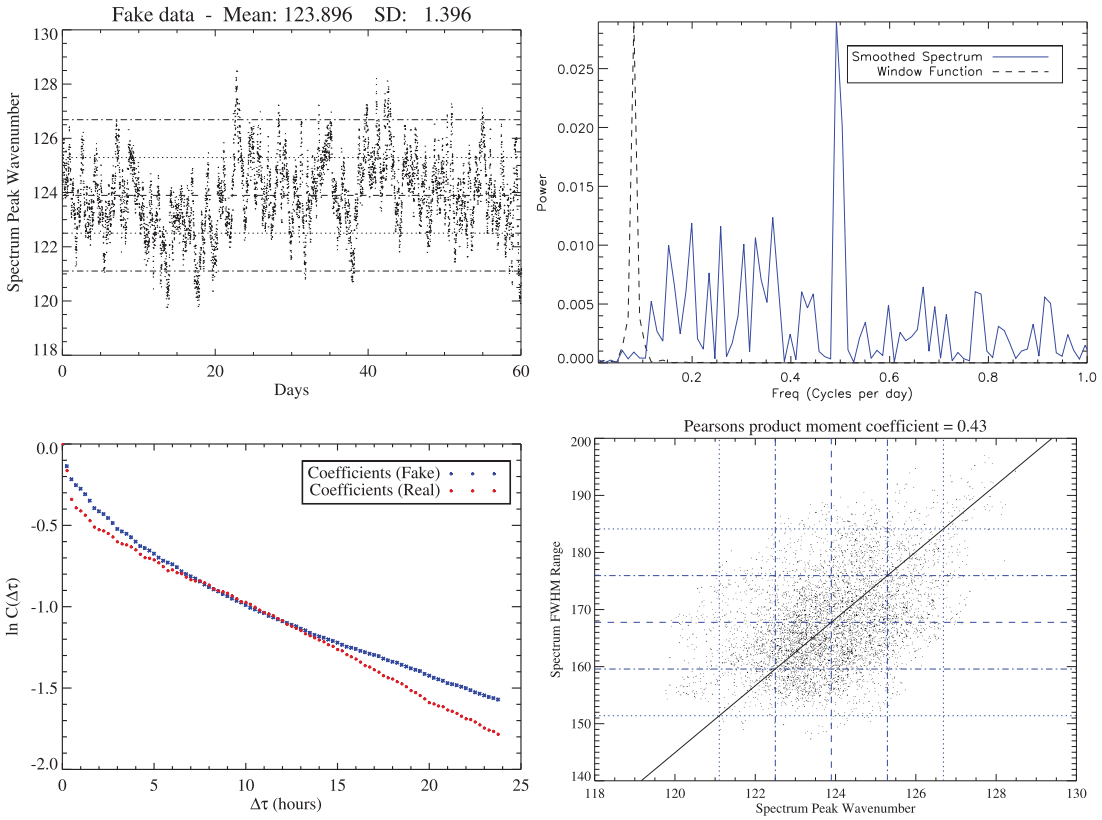

Figure 7 (Top-left) The peak wavenumbers for the supergranule feature in the spatial spectra derived from synthetic Dopplergrams (black dots) are smoothed with the same Savitzky–Golay filter as used for the MDI data. (Top-right) The frequency spectrum, similar to those in Figure 3, shows that, while a high background exists, there is a dominant peak of power at frequencies relating to a fluctuation period of around two days. (Bottom-left) Comparison of the time-evolution of correlation coefficients tracking supergranule patterns within synthetic (blue) and real (red) Doppler data. (Bottom-right) The cross-correlation of the peak wavenumber and the FWHM of the supergranule feature time-series give similar results to those derived from the MDI data.

is found to be $R_{\ell_{\rm peak}^{\rm FAKE},\Delta\ell^{\rm FAKE}} = 0.43$, where the respective mean and standard deviations for these two time-series are $\ell_{\rm peak}^{\rm FAKE} = 123.9 \pm 1.4$ and $\Delta\ell^{\rm FAKE} = 167.8 \pm 8.2$.

A toy model was constructed to simulate cumulative, uncorrelated exponential growth and decay patterns at random times. Performed over a number of iterations, a pattern emerges that is qualitatively similar to that of the MDI time-series (Figure 8). This simple model suggests that the fluctuations observed in the MDI data can be described by stochastic processes underlying the evolution of uncorrelated individual supergranules that comprise the global Doppler pattern.

7. Conclusions and Future Work

Time-series of globally averaged values for supergranule size, size-range, and horizontal velocity calculated from individual 15-minute-cadence MDI Doppler maps covering a time period of 60 days exhibit fluctuations with periods of three to five days. We found that the time-series for supergranule sizes are consistent between co-temporal MDI and HMI data, meaning that the observed fluctuations are solar in origin. While the source of these fluctu-

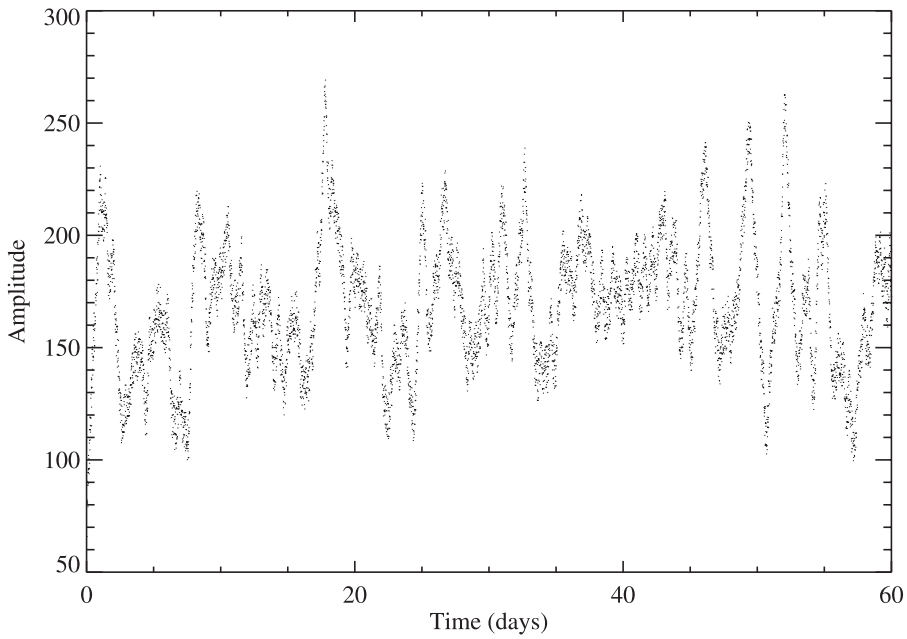

Figure 8 A time-series produced by the toy model of stochastic growth and decay of supergranulation has a similar appearance to that derived from MDI data.

ations is unclear, data simulations show that stochastic, uncorrelated variations seem to be qualitatively similar to the observational data.

Future studies of the time-evolution of the supergranulation pattern, including its growth and decay, may shed light on any influences underlying the time-series characteristics. This can include the adjustment of the input function that determines the pattern evolution within the data simulations to produce decay rates that more closely follow those seen within the real data.

With supergranulation being visible in other, non-Doppler datasets, such as Ca II K images, it is of interest to study whether these fluctuation patterns manifest in such data. McIntosh *et al.* (2011) highlighted variations in supergranulation properties within Ca II K images over long timescales at large time-steps, so it will be of interest to analyze these properties over shorter intervals with a more rapid cadence.

Acknowledgements This research was supported by an appointment to the NASA Postdoctoral Program at NASA Goddard Space Flight Center, administered by Oak Ridge Associated Universities through a contract with NASA via the *Solar Dynamics Observatory*. SDO is part of NASA's Living With a Star (LWS) program. HMI was designed and assembled at Stanford University and Lockheed Martin Solar and Astrophysics Laboratory. SOHO is a project of international cooperation between ESA and NASA. The authors extend their gratitude to John Beck of Stanford University for producing the de-rotated Dopplergram datasets. We also thank the referee for the constructive comments that have improved the content of this article.

References

Goldbaum, N., Rast, M.P., Ermolli, I., Sands, J.S., Berrilli, F.: 2009, The intensity profile of the solar supergranulation. *Astrophys. J.* **707**, 67 – 73. doi:10.1088/0004-637X/707/1/67.

Hart, A.B.: 1956, Motions in the Sun at the photospheric level. IV. The equatorial rotation and possible velocity fields in the photosphere. *Mon. Not. Roy. Astron. Soc.* **116**, 38.

Hathaway, D.H.: 1988a, Simulating photospheric Doppler velocity fields. *Solar Phys.* **117**, 329 – 341. doi:10.1007/BF00147251.

Hathaway, D.H.: 1988b, Temporal filters for isolating steady photospheric flows. *Solar Phys.* **117**, 1 – 12. doi:10.1007/BF00148567.
Hathaway, D.H.: 1992, Spherical harmonic analysis of steady photospheric flows. II. *Solar Phys.* **137**, 15 – 32. doi:10.1007/BF00146573.
Hathaway, D.H., Beck, J.G., Bogart, R.S., Bachmann, K.T., Khatri, G., Petitto, J.M., Han, S., Raymond, J.: 2000, The photospheric convection spectrum. *Solar Phys.* **193**, 299 – 312. doi:10.1023/A:1005200809766.
Hathaway, D.H., Beck, J.G., Han, S., Raymond, J.: 2002, Radial flows in supergranules. *Solar Phys.* **205**, 25 – 38. ADS:2002SoPh..205...25H, doi:10.1023/A:1013881213279.
Hathaway, D.H., Williams, P.E., Dela Rosa, K., Cuntz, M.: 2010, The advection of supergranules by the Sun's axisymmetric flows. *Astrophys. J.* **725**, 1082 – 1090. doi:10.1088/0004-637X/725/1/1082.
Hindman, B.W., Gizon, L., Duvall, T.L. Jr., Haber, D.A., Toomre, J.: 2004, Comparison of solar subsurface flows assessed by ring and time-distance analyses. *Astrophys. J.* **613**, 1253 – 1262. doi:10.1086/423263.
Korzennik, S.G., Rabello-Soares, M.C., Schou, J.: 2004, On the determination of Michelson Doppler Imager high-degree mode frequencies. *Astrophys. J.* **602**, 481 – 516. doi:10.1086/381021.
Leighton, R.B., Noyes, R.W., Simon, G.W.: 1962, Velocity fields in the solar atmosphere. I. Preliminary report. *Astrophys. J.* **135**, 474. doi:10.1086/147285.
Liu, Y., Norton, A.A.: 2001, Mdi measurement errors: the magnetic perspective, SOI technical note. Technical report, Stanford University.
Mandelbrot, B.B., Wallis, J.R.: 1969, Some long-run properties of geophysical records. *Water Resour. Res.* **5**, 321 – 340. doi:10.1029/WR005i002p00321.
McIntosh, S.W., Leamon, R.J., Hock, R.A., Rast, M.P., Ulrich, R.K.: 2011, Observing evolution in the supergranular network length scale during periods of low solar activity. *Astrophys. J. Lett.* **730**, L3. doi:10.1088/2041-8205/730/1/L3.
Meunier, N., Roudier, T., Rieutord, M.: 2008, Supergranules over the solar cycle. *Astron. Astrophys.* **488**, 1109 – 1115. doi:10.1051/0004-6361:20078835.
Meunier, N., Tkaczuk, R., Roudier, T., Rieutord, M.: 2007, Velocities and divergences as a function of supergranule size. *Astron. Astrophys.* **461**, 1141 – 1147. doi:10.1051/0004-6361:20065625.
Pesnell, W.D.: 2012, Solar cycle predictions (invited review). *Solar Phys.* **281**, 135. doi:10.1007/s11207-012-9997-5.
Plaskett, H.H.: 1916, A variation in the solar rotation. *Astrophys. J.* **43**, 145. doi:10.1086/142239.
Plaskett, J.S., Delury, R.E.: 1913, The solar rotation in 1911. *Astrophys. J.* **37**, 73. doi:10.1086/141979.
Rieutord, M., Rincon, F.: 2010, The Sun's supergranulation. *Living Rev. Solar Phys.* **7**, 2. doi:10.12942/lrsp-2010-2
Rieutord, M., Roudier, T., Rincon, F., Malherbe, J.-M., Meunier, N., Berger, T., Frank, Z.: 2010, On the power spectrum of solar surface flows. *Astron. Astrophys.* **512**, A4. doi:10.1051/0004-6361/200913303.
Scherrer, P.H., Bogart, R.S., Bush, R.I., Hoeksema, J.T., Kosovichev, A.G., Schou, J., Rosenberg, W., Springer, L., Tarbell, T.D., Title, A., Wolfson, C.J., Zayer, I., MDI Engineering Team: 1995, The solar oscillations investigation – Michelson Doppler Imager. *Solar Phys.* **162**, 129 – 188. doi:10.1007/BF00733429.
Schou, J., Antia, H.M., Basu, S., Bogart, R.S., Bush, R.I., Chitre, S.M., Christensen-Dalsgaard, J., di Mauro, M.P., Dziembowski, W.A., Eff-Darwich, A., Gough, D.O., Haber, D.A., Hoeksema, J.T., Howe, R., Korzennik, S.G., Kosovichev, A.G., Larsen, R.M., Pijpers, F.P., Scherrer, P.H., Sekii, T., Tarbell, T.D., Title, A.M., Thompson, M.J., Toomre, J.: 1998, Helioseismic studies of differential rotation in the solar envelope by the solar oscillations investigation using the Michelson Doppler Imager. *Astrophys. J.* **505**, 390 – 417. doi:10.1086/306146.
Thompson, W.T.: 2002, Standardized coordinate systems for solar image data. *Adv. Space Res.* **29**, 2093 – 2098. doi:10.1016/S0273-1177(02)00155-2.
Williams, P.E., Pesnell, W.D.: 2011a, Comparisons of supergranule characteristics during the solar minima of Cycles 22/23 and 23/24. *Solar Phys.* **270**, 125 – 136. doi:10.1007/s11207-011-9718-5.
Williams, P.E., Pesnell, W.D.: 2011b, Properties of supergranulation during the solar minima of Cycles 22/23 and 23/24. *J. Phys.* **CS-271**(1), 012082. doi:10.1088/1742-6596/271/1/012082.
Williams, P.E., Pesnell, W.D., Beck, J.G., Lee, S.L.: 2013, Comparative studies of supergranule characteristics using SDO/HMI and SOHO/MDI Dopplergrams. *Solar Phys.*, doi:10.1007/s11207-013-0330-8.